Particles II

Access the latest eBook →

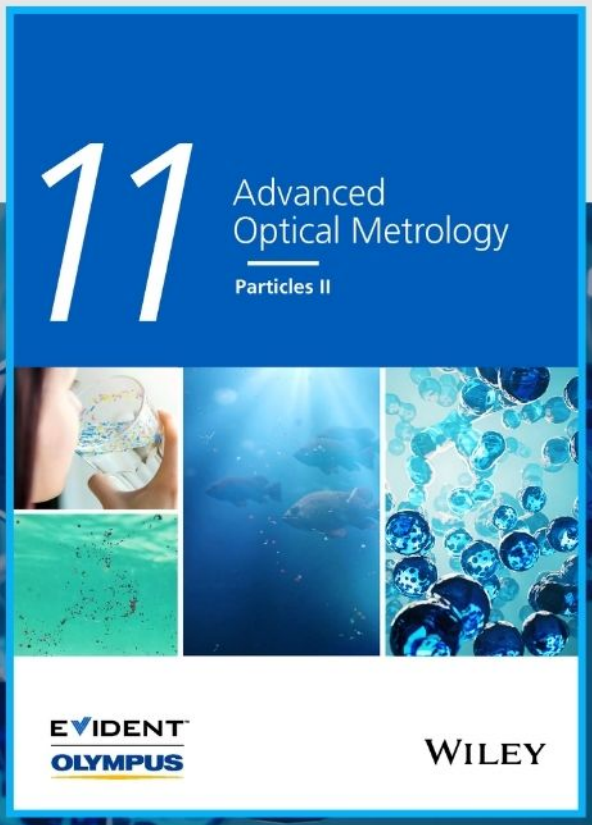

Impact on Biological Systems and the Environment

This eBook is dedicated to the research of Professor David Wertheim.
In collaboration with various groups, Professor Wertheim uses confocal microscopy to analyse the impact of different types of particles on human health and the environment, with a focus on human health-hazardous particles detected with solid-state nuclear track detectors (SSNTD). Download for free, today.

EVIDENT
OLYMPUS

WILEY

Reversible Pressure-Dependent Mechanochromism of Dion–Jacobson and Ruddlesden–Popper Layered Hybrid Perovskites

Loreta A. Muscarella, Algirdas Dučinskas, Mathias Dankl, Michał Andrzejewski, Nicola Pietro Maria Casati, Ursula Rothlisberger, Joachim Maier, Michael Graetzel, Bruno Ehrler, and Jovana V. Milić**

Layered Dion–Jacobson (DJ) and Ruddlesden–Popper (RP) hybrid perovskites are promising materials for optoelectronic applications due to their modular structure. To fully exploit their functionality, mechanical stimuli can be used to control their properties without changing the composition. However, the responsiveness of these systems to pressure compatible with practical applications (<1 GPa) remains unexploited. Hydrostatic pressure is used to investigate the structure–property relationships in representative iodide and bromide DJ and RP 2D perovskites based on 1,4-phenylenedimethylammonium (PDMA) and benzylammonium (BzA) spacers in the 0–0.35 GPa pressure range. Pressure-dependent X-ray scattering measurements reveal that lattices of these compositions monotonically shrink and density functional theory calculations provide insights into the structural changes within the organic spacer layer. These structural changes affect the optical properties; the most significant shift in the optical absorption is observed in $(BzA)_2PbBr_4$ under 0.35 GPa pressure, which is attributed to an isostructural phase transition. Surprisingly, the RP and DJ perovskites behave similarly under pressure, despite the different binding modes of the spacer molecules. This study provides important insights into how the manipulation of the crystal structure affects the optoelectronic properties of such materials, whereas the reversibility of their response expands the perspectives for future applications.

1. Introduction

Layered 2D hybrid perovskites have attracted considerable interest due to their unique optoelectronic properties and highly modular structure that can be tailored by altering both organic and inorganic components.[1–4] These materials are composed of organic spacer (S) layers connecting adjacent perovskite slabs based on the $S_xA_{n-1}M_nX_{3n+1}$ formula, where x is the number of spacer molecules connecting two neighboring perovskite layers. This involves a central (A) cation (e.g., Cs^+, methylammonium (MA^+), formamidinium (FA^+), etc.) embedded in the $\{MX_6\}$ octahedral metal–halide framework based on divalent metal ions (Pb^{2+} or Sn^{2+}) and halide (X^-) anions (I^-, Br^-, or Cl^-). Their structural characteristics are the result of a subtle interplay between the organic spacer layer and the inorganic slabs and they are often broadly classified into Ruddlesden–Popper (RP)[4,5] and Dion–Jacobson (DJ) phases.[6] In the case

L. A. Muscarella, B. Ehrler
Center for Nanophotonics
AMOLF
Science Park 104, Amsterdam XG 1098, The Netherlands
E-mail: b.ehrler@amolf.nl

A. Dučinskas, M. Graetzel, J. V. Milić
Laboratory of Photonics and Interfaces
Institute of Chemical Sciences and Engineering
École Polytechnique Fédérale de Lausanne
Lausanne CH-1015, Switzerland

A. Dučinskas, J. Maier
Max Planck Institute for Solid State Research
Heisenbergstr. 1, 70569 Stuttgart, Germany

M. Dankl, U. Rothlisberger
Laboratory of Computational Chemistry and Biochemistry
Institute of Chemical Sciences and Engineering
École Polytechnique Fédérale de Lausanne
Lausanne CH-1015, Switzerland

M. Andrzejewski, N. P. M. Casati
Paul Scherrer Institute
Forschungsstrasse 111, Villigen CH-5232, Switzerland

J. V. Milić
Adolphe Merkle Institute
University of Fribourg
Fribourg CH-1700, Switzerland
E-mail: jovana.milic@unifr.ch

The ORCID identification number(s) for the author(s) of this article can be found under https://doi.org/10.1002/adma.202108720.

DOI: 10.1002/adma.202108720

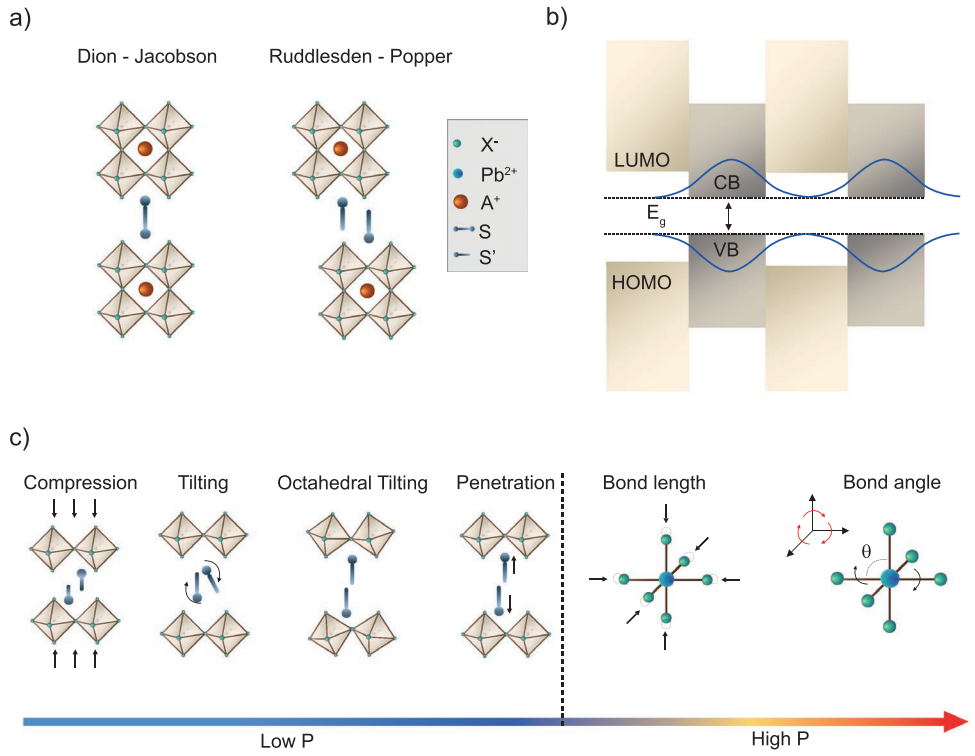

Figure 1. a) Schematic representation of Dion–Jacobson (DJ) and Ruddlesden–Popper (RP) phases and b) their quantum well structure, with the energy bandgap (E_g) defined by conduction band (CB) and valence band (VB) edges of the inorganic slabs and the highest occupied (HOMO) and lowest unoccupied (LUMO) molecular orbitals of the organic spacer layer. In blue, the electronic wavefunction is shown, located mostly in the inorganic framework. c) Illustration of the different possible structural changes that control the optoelectronic properties of layered (2D) perovskites by external pressure: at low pressure, the main effect is reflected in the changes in the organic spacer and octahedral tilting, whereas at high pressure an additional effect on the bond length and angle is expected. A representative RP perovskite is used in the illustration. *P* = pressure.

of RP perovskites, the perovskite layers are displaced by half the length of the unit cell vectors along the in-plane direction, which mostly involves monofunctional spacers ($x = 2$),[3] whereas DJ perovskites attain the alignment in the structure without relative displacement and are commonly based on bifunctional spacer molecules ($x = 1$; **Figure 1**a).[7] The monofunctional spacers in RP phases form bilayers with a van der Waals gap,[8] whereas bifunctional spacers in DJ layered perovskites directly connect the neighboring perovskite slabs.[6] They are further classified based on the number of perovskites layers (n) that are separated by the organic spacers (e.g., $n = 1, 2, 3$, etc.).[2,3,6] Since the spacers are mostly electronically insulating, the charge carriers in these materials are predominantly confined to the inorganic slabs, resulting in natural quantum well (QW) behavior (Figure 1b), where optical bandgap decreases with the increasing width of the QW because of reduced quantum confinement.[9,10] This implies that their optical properties can be modulated by changing the number of perovskite layers (n). Furthermore, quantum confinement can be tuned by the width of the potential barrier, which is controlled by the spacer size that further affects their optoelectronic properties.[11,12]

It would be of interest to control these effects on the potential barrier width without changing the perovskite composition, which can be achieved by relying on their mechanical properties and responsiveness to external stimuli, such as pressure.[13,14] Thus, understanding the structure–property relationships in such layered perovskites can serve as a guide to design materials with specific properties, whereas understanding the behavior of $n = 1$ layered 2D perovskites provides a limiting case for the analysis of $n > 1$ systems. Moreover, knowing the pressure response of these materials might open opportunities for sensing applications, where sensitivity to external mechanical stimuli and reversibility are highly desirable. This is also relevant in other contexts, such as for flexible solar cells, where strain might be induced during operation.

The relatively low bulk modulus (K) of hybrid 3D perovskites (of the order of tens of GPa) renders them soft materials that are more easily compressible across different pressure ranges, demonstrating mechanochromic behavior.[15–19] For comparison, halide perovskites show at least a five times smaller bulk modulus than their oxide analogs (with $K > 100$ GPa).[20,21] For 2D hybrid halide perovskites, the bulk modulus might not be an appropriate descriptor of their mechanical properties since compression in these materials is mostly anisotropic.[14,22] Alternatively, their mechanical properties can be better described by in-plane or out-of-plane Young's modulus (E),[23] which is more commonly used for layered perovskites as it defines the material's ability to deform along a given axis when force is applied. In-plane E is typically determined by the M–X bond strength, whereas out-of-plane E depends on the organic spacer.[3,24,25] An appropriate choice of organic spacers can lead to a much smaller E in the 2D layered hybrid perovskites than the 3D analogous,[24,25] suggesting a higher pressure sensitivity for tuning their optoelectronic and transport properties. The

anisotropy of layered hybrid perovskites renders their compression predominant in out-of-plane (*a*-axis) direction under pressure.[14,22,26] This is expected to be mainly determined by the organic spacer layer and it could result in different structural changes, including the compression and tilting of the organic spacer, and increased penetration depth, also inducing possible changes in the octahedral tilting of the inorganic layer (Figure 1c, left). These structural distortions are expected to change the QW structure or the M and X orbital overlaps and, consequently, optical properties. More specifically, the compression of spacer molecules or M–X bonds lowers the optical bandgap due to increased overlap of wave functions between adjacent perovskite layers or increased antibonding atomic overlap between the metal and halide orbitals, respectively. The deviation of M–X–M angle from the 180° (i.e., octahedral tilting) leads to an opposite effect.[27] Under higher pressures, the compressed inorganic perovskite lattice relaxes through two competing processes, namely M–X bond tilting or M–X bond contraction (Figure 1c, right),[7,28,29] which directly affect the optoelectronic properties.[13,28]

While previous work primarily involved the behavior of hybrid perovskites under high pressure,[13,28] it is of great importance to study effects in mild pressure regimes (<1 GPa), since induced levels of strain are comparable with polaron effects,[30,31] chemical (i.e., conformational) strain,[32,33] or strain due to lattice mismatches,[33,34] especially in 2D/3D perovskite composites.[35] In that regard, the behavior under mild pressures may serve as a powerful tool for controlling the properties of these materials in a manner comparable to other processes inducing internal strain. However, the investigations of layered 2D perovskites in such mild-pressure ranges are underrepresented and the differences in the pressure-dependent behavior of RP and DJ phases remain elusive.

Herein, we investigated representative DJ and RP 2D perovskites based on 1,4-phenylenedimethylammonium (PDMA) and benzylammonium (BzA) spacers under hydrostatic pressure up to 0.35 GPa. These aromatic spacer moieties are closely comparable, and they have already demonstrated the capacity to form well-defined 2D perovskite phases,[27,36,37] which makes them appropriate models to analyze the differences in compression between RP and DJ type perovskites. We further study the effect of the halide counter ion comparing systems based on $(BzA)_2PbX_4$ and $(PDMA)PbX_4$ compositions for X = I, Br ions by means of pressure-dependent UV–vis absorption, photoluminescence spectroscopy, and X-ray scattering measurements, as well as density functional theory (DFT) calculations. One might expect that the additional degrees of freedom in RP spacer layers would render them more compressible as compared to their DJ analogs. Similarly, the differences in the lattice compression of I- and Br-based systems are expected.[27] Instead, we find that the bulk moduli of RP and DJ are comparable under mild pressure despite the different binding mode of the spacers. The compression is predominant along the stacking direction (*a*-axis). In addition, we establish no direct pressure-dependent difference between the I- and Br-based compositions as their differences under pressure are more subtle. For all compositions, we observe that the unit cell monotonically shrinks with the applied pressure, which is accompanied by a red shift of the optical absorption upon increasing the pressure to 0.35 GPa. Moreover, $(BzA)_2PbBr_4$ shows the most significant red shift of the optical absorption (–54.9 meV) as compared to the other compositions where a comparable shift (≈30 meV) is observed. Synchrotron diffraction measurements and DFT calculations suggest that this is due to the smaller lattice spacing of the Br-based perovskite planes that initially enables only a shallow penetration of the BzA cations into the inorganic layer, but leads to a stronger pressure response with larger structural rearrangements as compared to I- and PDMA-based DJ analogs. The pressure responses are found to be reversible, stimulating future applications.

2. Results and Discussion

To gain insights into the pressure response of RP and DJ perovskites, we prepared I- and Br-based precursor solutions using the monofunctional BzA and the bifunctional PDMA as organic spacers.[8,27,36–38] These aromatic spacers were selected based on their comparable structural features that permit the formation of phase-pure 2D RP and DJ perovskites. We fabricated thin films based on $(PDMA)PbX_4$ and $(BzA)_2PbX_4$ (X = I, Br) compositions, as described in the Methods Section of the Supporting Information. We focused the analysis on the 2D systems of $n = 1$ composition, since they represent the most well-defined layered structures that are typically oriented parallel with respect to the substrate.[2,3,9]

Layered perovskite structure in the given thin films is confirmed by well-defined periodic diffraction patterns measured by X-ray diffraction (XRD) at ambient pressure, which exhibit the (h00) reflections that confirm parallel orientation of the perovskite slabs with respect to the substrate (**Figure 2**). A shift toward higher angles is observed when the iodide in the PDMA-based system is replaced by the bromide counter ion (Figure 2a), in accordance with the smaller halide radius, which in turn led to a smaller unit cell. On the contrary, when the iodide is replaced by bromide in the BzA-based systems, we observe the opposite behavior and a shift toward lower angles, indicating a larger lattice parameter (Figure 2b). This finding could suggest a difference in the packing of the spacer for different halide counter ions, implying a larger distance between the perovskites slabs in $(BzA)_2PbBr_4$ as compared to the iodide counterpart.

To understand this behavior as a function of halide counter ion and to elucidate the role of the physical pressure on the structural properties of these compositions, we investigated pressure-induced changes in the lattice parameters by pressure-dependent X-ray scattering (Figure S1,S2, Supporting Information). Diffraction data of perovskite powders for each composition were acquired using a synchrotron source at several pressure points in a membrane diamond-anvil cell (experimental details and the attribution of the diffraction peaks are provided in the Experimental Methods and Note 1, Supporting Information). At low pressures, the monoclinic $P2_1/c$ space group is assigned to $(PDMA)PbI_4$ and $(PDMA)PbBr_4$, the orthorhombic *Pcab* with non-standard settings of *Pbca* in order to keep consistency the organic spacers along [100] direction to $(BzA)_2PbI_4$, and the orthorhombic $Cmc2_1$ to $(BzA)_2PbBr_4$. Despite compression along all the axes (**Figure 3**a,b), the largest compression is

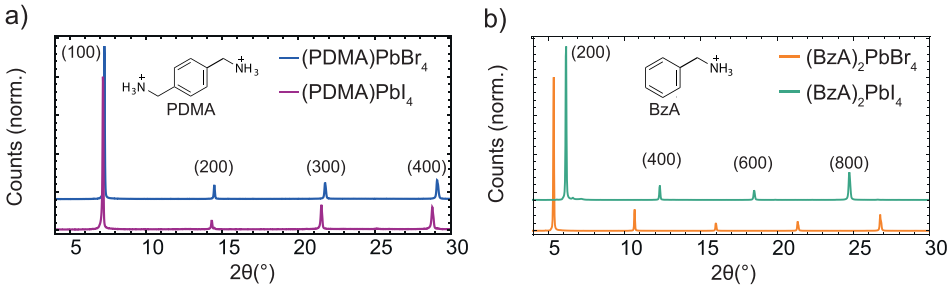

Figure 2. a,b) X-ray diffraction pattern (Cu Kα 1.5406 Å) of thin films based on (PDMA)PbX_4 (a) and $(BzA)_2PbX_4$ (b) (X = I, Br) compositions on microscope glass slides at ambient pressure.

found to be along the *a*-axis (i.e., stacking direction) for all systems, which is in accordance with previous reports.[22,26] This trend is significantly more pronounced for the $(BzA)_2PbBr_4$ (Figure 3b), which is the only one among the studied compositions that features a non-centrosymmetric structure. It shows a larger compression in the stacking direction (–6% relative change) and an elongation of the in-plane lattice parameters (*b*- and *c*-axes) followed by a compression (Figure S3, Supporting Information)—a rare structural feature known as negative area compressibility. Furthermore, non-centrosymmetric $(BzA)_2PbBr_4$ crystal structure reveals two distinct values of Pb–X–Pb angles (ϕ_1 and ϕ_2 in the *b*–*c* plane), whereas the octahedral tilting in the other three compositions is defined by single Pb–X–Pb angle (ϕ_1; as shown in $(BzA)_2PbI_4$, Figure 3c). Perovskite layers are more distorted in $(BzA)_2PbBr_4$ composition since the deviation of ϕ_1 and ϕ_2 from 180° is larger as compared to its iodide analog (Figure 3d). Therefore, the cavities between the octahedra are smaller, which in turn hinders the penetration of organic spacer into the perovskite layers leading to the higher interlayer spacing in $(BzA)_2PbBr_4$ (Figure 2b). The angle between two adjacent octahedra hardly changes under pressure in the case of $(BzA)_2PbI_4$, whereas both Pb–Br–Pb angles in $(BzA)_2PbBr_4$ change significantly between 0.15 and 0.25 GPa, the range where the compression along the *a*-axis is the strongest (Figure 3d). Although these changes are remarkable, the $Cmc2_1$ space group is preserved, implying that $(BzA)_2PbBr_4$ undergoes an isostructural phase transition in this pressure range.[39]

To quantify at a first approximation the compressibility of the compositions in study, we calculate the isothermal bulk modulus, which is the inverse of compressibility, from the pressure–volume relationship assuming mostly isotropic response to pressure by relying on the second-order Birch–Murnaghan equation of state (Note 2, Supporting Information).[40] As a

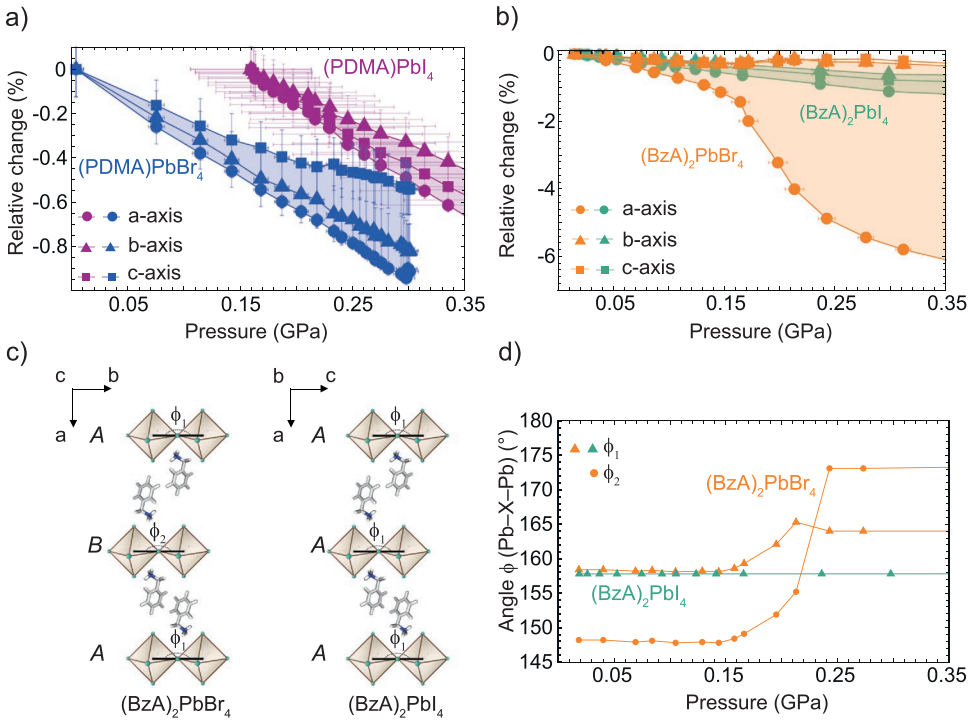

Figure 3. a,b) Relative change of the lattice parameters as a function of pressure for (PDMA)PbX_4 (a) and $(BzA)_2PbX_4$ (b) compositions (X = I, Br). c) Schematic representation of $(BzA)_2PbBr_4$ alternating inorganic sheet (ABA) in comparison with its iodide counterpart (AAA) and d) the corresponding inter-octahedral tilting angles in the $(BzA)_2PbBr_4$ and $(BzA)_2PbI_4$ systems, as extracted from the refinement of X-ray powder diffraction measurements.

result, there was no effect of the halide ion in PDMA-based systems since both (PDMA)PbI_4 and (PDMA)$PbBr_4$ show comparable bulk moduli (Figure S4a, Supporting Information). Furthermore, van der Waals gap renders both $(BzA)_2PbI_4$ and $(BzA)_2PbBr_4$ slightly more compressible (i.e., having lower bulk moduli) as compared to PDMA-based systems (Figure S4b, Supporting Information). In addition, two distinct bulk moduli for $(BzA)_2PbBr_4$ composition have been identified, which are attributed to isostructural phases at low and elevated pressure.[41] These results (Table S2, Supporting Information) suggest the important role of the spacer cation in the resulting behavior. Since elucidating the local orientation of the organic spacer molecules remains challenging based on the X-ray powder diffraction data, we further investigate the effect of pressure on the organic spacer layer by DFT calculations.

For DFT calculations, the data obtained from the synchrotron scattering measurements was used as initial starting point. For each pressure the coordination of the atoms were relaxed without any constraints while fixing the lattice parameters at the experimentally measured values in order to better account for the thermal expansion of the lattice parameters at the measured temperature. The results suggest that the compression along the *a*-axis is due to reduced distance between the two neighboring spacers and their closer packing (**Figure 4**). The initial vertical distance between the two BzA spacers, *d*(BzA–BzA), defined from the center of the benzyl ring, is significantly larger in the case of $(BzA)_2PbBr_4$ (4.43 Å) as compared to $(BzA)_2PbI_4$ (2.97 Å). This distance decreases by 0.4 Å for $(BzA)_2PbBr_4$, whereas for the I-based analog the decrease accounts to only 0.08 Å within the same pressure range, resulting in a larger compression for $(BzA)_2PbBr_4$ (Figure 4a). Calculations further suggest the presence of two distinct octahedra tilting angles (141.5° and 154.5°) in $(BzA)_2PbBr_4$ (Figure S5a, Supporting Information). These angles are lower than the one in $(BzA)_2PbI_4$ (by 4° and 16°, respectively), which represents a higher distortion of the octahedra, thereby leaving less room for the BzA spacers to penetrate than the already shorter Pb–Br distances would allow. The penetration depth of the spacer into the inorganic framework is the result of an interplay of interactions between the organic and inorganic components and it changes continuously upon increasing pressure for the PDMA-based compositions and $(BzA)_2PbI_4$ (Figure S5b, Supporting Information), whereas in $(BzA)_2PbBr_4$ there is an abrupt change leading to higher penetration depth (Figure 4b). This difference in the $(BzA)_2PbBr_4$ system could primarily originate from the changes in the octahedral tilting angles, the spacer packing and orientation, and the penetration depth into the inorganic framework.[27] In addition to the penetration of the spacer, the Pb–X bond length could potentially also change under pressure. The equatorial Pb–Br bond lengths in $(BzA)_2PbBr_4$ at low pressure (2.98 and 3.02 Å) are smaller than the ones in $(BzA)_2PbI_4$ (3.21 and 3.25 Å; Figure S5c, Supporting Information), leading to a denser octahedral packing and, in turn, a significantly lower penetration into the Pb–Br lattice at ambient pressure. These structural differences in the low-pressure regime also translate into different responses to external pressure. However, the axial Pb–X bond lengths remain constant over the entire pressure range (Figure S5c, Supporting Information). DFT calculations suggest a very small compression of Pb–X bonds with pressure that can affect the Pb–X antibonding overlap and thereby the bandgap, which has not been detected experimentally. This implies that the measured compressions are not caused by the changes in the Pb–X bond lengths. Instead, the response to mild pressure is the result of changes in the packing within the organic spacer layer (Figure S6, Supporting Information). This packing within the organic spacer layer has been previously associated with the non-centrosymmetric structure of the $(BzA)_2PbBr_4$ composition,[27] which is unique for this composition as compared to others. The calculations for $(BzA)_2PbI_4$ and (PDMA)PbX_4 show comparable change under pressure, whereas the two BzA spacers in $(BzA)_2PbBr_4$ were found to move closer together (Tables S3–S6, Supporting Information). In the pressure range between 0.164 to 0.213 GPa, the BzA spacers were found to penetrate deeper into the inorganic lattice, hence affecting the resulting properties (Figure 4b). This process is accompanied by a decrease in the BzA tilting angle, defined as the angle between the *a*-axis and the benzyl plane (Figure S5d, Supporting Information). Such a change corresponds to a rearrangement of the BzA spacers into a more parallel orientation with respect to the *a*-axis. Moreover, this is reflected in the changes in the horizontal direction that are uniquely observed for the $(BzA)_2PbBr_4$ composition (Figure S5e, Supporting Information). Consequently, the significant change in the distance between the neighboring BzA groups is qualitatively in accordance with the experimental observation of a larger compression for $(BzA)_2PbBr_4$. Such changes in the

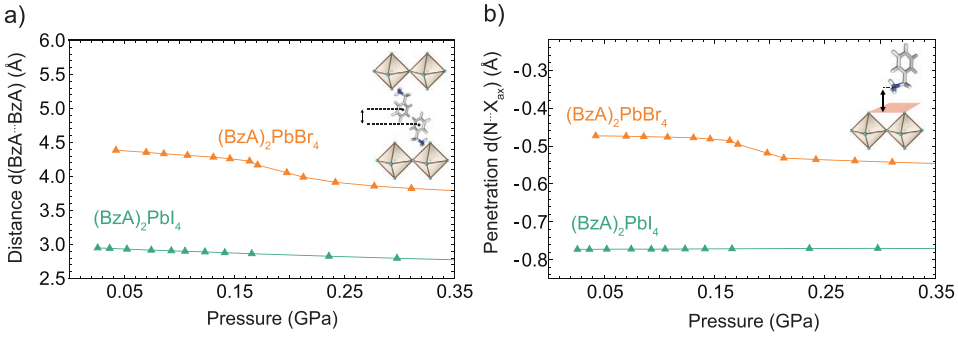

Figure 4. a) Calculated average distances of the (vertically) neighboring BzA rings *d*(BzA···BzA) in the RP layer and b) nitrogen penetration depth in the halide plane $d(N\cdots X_{ax})$ as a measure of the penetration depth based on the DFT-optimized structures (PBEsol). The zero is set at the halide planes and larger penetration corresponds to more negative values.

assembly of the spacer layer in response to pressure are further reflected in their optoelectronic properties.

To assess the mechanochromic properties, we monitored the optical absorption as a function of applied external stress of $(PDMA)PbX_4$ and $(BzA)_2PbX_4$ (X = Br, I). The samples were placed inside a hydrostatic pressure cell filled with an inert liquid (tetradecafluorohexane, FC-72, as detailed in the Methods Section of the Supporting Information and schematically depicted in **Figure 5**a), which exposes the material to isotropic pressure excluding the effects of its orientation with respect to the surface. We applied pressure from 0 to 0.35 GPa in steps of 0.05 GPa through a manual pump. Quantum and dielectric confinement effects give rise to an intense and narrow excitonic absorption feature (Figure S7, Supporting Information), typical of layered 2D perovskites.[42,43] We observe a continuous shift of the excitonic peak toward lower energies for all analyzed perovskite compositions (Figure 5b–e). In addition, the red shift confirms that a mild external pressure can be sufficient to tune the optical properties in these materials. Similarly, pressure-dependent PL measurements show a redshift upon increasing pressure (Figure S8, Supporting Information). We obtained the excitonic peak energy of the $(PDMA)PbI_4$ and $(BzA)_2PbI_4$ as a function of pressure fitting a skewed Gaussian function to the absorption spectra. At ambient pressure, the excitonic peak energy of $(PDMA)PbI_4$ and $(BzA)_2PbI_4$ is 2.41 and 2.36 eV, respectively. Upon increasing the pressure, the excitonic-peak shift at 0.30 GPa as compared to ambient pressure is about (-25 ± 0.6) meV for $(PDMA)PbI_4$ and (-27 ± 1) meV for $(BzA)_2PbI_4$ (Figure 5f). We observed a similar linear trend for both RP and DJ perovskites until the pressure of 0.30 GPa, where the response to external pressure causes a comparable energy shift. For pressures higher than 0.3 GPa,

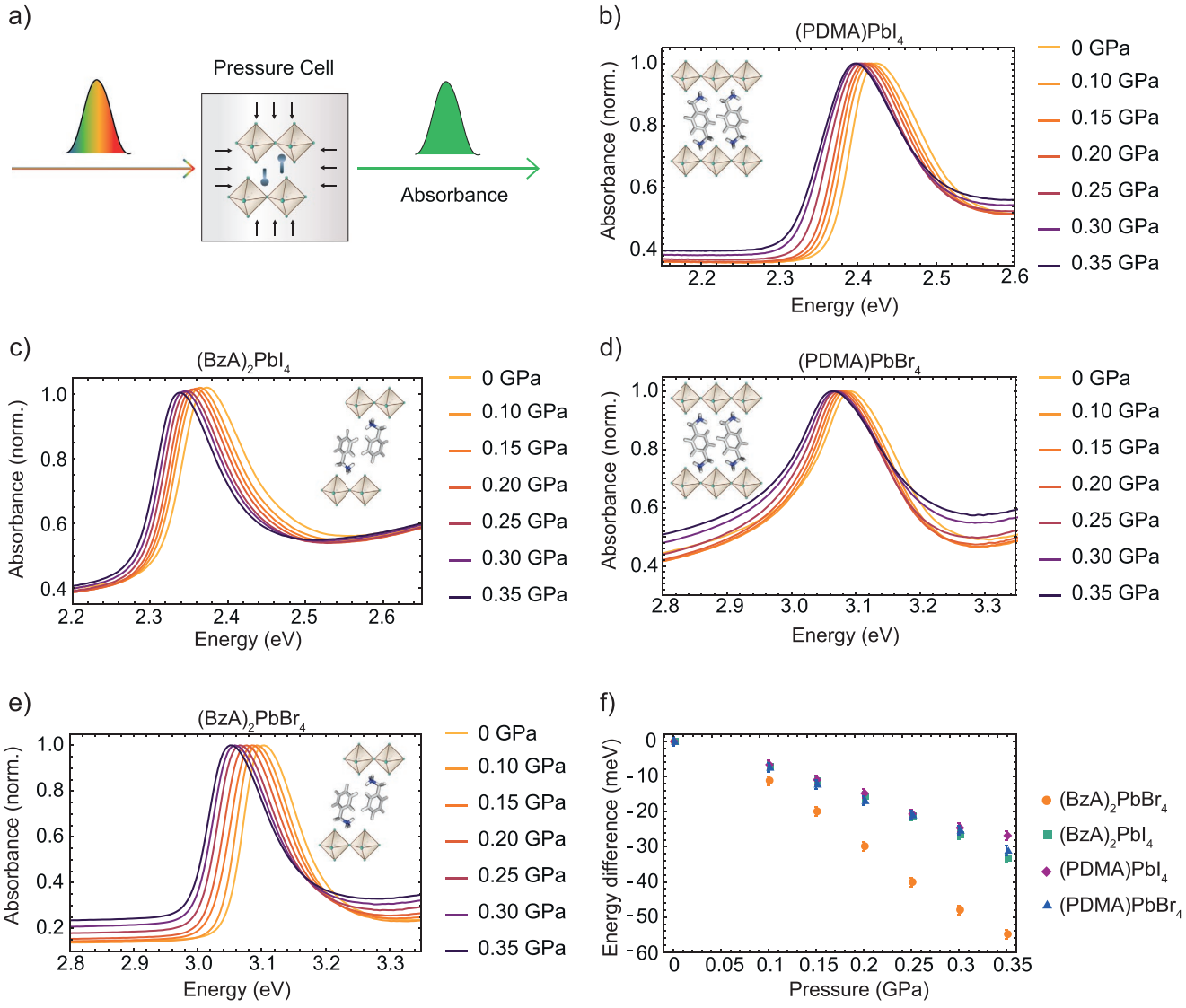

Figure 5. a) Schematic of the experimental setup for pressure-dependent absorbance measurements and b–e) pressure-dependent absorbance for $(PDMA)PbI_4$ (b), $(BzA)_2PbI_4$ (c), $(PDMA)PbBr_4$ (d), and $(BzA)_2PbI_4$ (e) in the pressure range from ambient to 0.35 GPa. The inset shows a schematic representation of the layered structures. f) Energy difference of the excitonic peak energy as a function of applied pressure.

the $(BzA)_2PbI_4$ appears to shift to a larger extent in comparison with the $(PDMA)PbI_4$, showing an energy shift of (−33 ± 1) and (−27 ± 0.5) meV, respectively. A more pronounced difference in the response for higher pressures (above 0.3 GPa) is likely to be associated with the structural differences of the corresponding RP and DJ phases, in accordance with the previous reports.[22–26] Further investigations at pressures above 0.35 GPa are not possible with the same experimental setup because of the limitations of the hydrostatic pressure cell. Nevertheless, monitoring the shift of the excitonic peak by its maximum intensity reveals the same slope as fitting the skewed Gaussian with a larger error given by the resolution of the absorbance measurement (Figure S9 and Tables S7–S10, Supporting Information). For Br-based analogues, the excitonic peak energy is 3.06 and 3.07 eV for $(PDMA)PbBr_4$ and $(BzA)_2PbBr_4$, respectively. Upon increasing the pressure to 0.35 GPa, the energy shifts for both $(PDMA)PbBr_4$ and $(BzA)_2PbBr_4$ by (−31 ± 1) and (−55 ± 0.2) meV, respectively. The $(BzA)_2PbBr_4$ has a notably larger energy shift than its I- and PDMA-based systems (Figure 5f and Tables S11–S14, Supporting Information).

To sum up, the energy shifts in I-based samples closely correspond to each other, which suggests that pressure-dependent properties are comparable for RP and DJ phases in this pressure range. However, Br-based systems show contrasting differences, with $(BzA)_2PbBr_4$ having substantially larger shifts as compared to $(PDMA)PbBr_4$ and I-based systems. Such shift in $(BzA)_2PbBr_4$ is in accordance with the more significant compressibility as compared to its I-based and PDMA-based systems (Figure S4, Supporting Information). Furthermore, the isostructural phase transition induced by the reduction of octahedral tilting (i.e., the Pb–Br–Pb angle is closer to 180°) is associated with the change of penetration depth of the BzA spacers into the perovskite lattice and the distance between the neighboring spacers. This is related to the quantum confinement, which is reduced by the change in potential barrier width. The qualitative variations of the bandgaps as a function of pressure are well reproduced theoretically (Figure S10, Supporting Information).

We can directly correlate the experimental structural parameters obtained by pressure-dependent XRD measurements with the changes in the optical absorption. The relationship between the shift in the exciton absorption peak and the length of the *a*-axis is linear for both PDMA-based and BzA-based samples (**Figure 6**), with the exception in $(BzA)_2PbBr_4$, where we observe two different regimes that are attributed to the isostructural phase transition. A linear fit of the energy shift as a function of the *a*-axis length results in a comparable slope of 0.223 ± 0.009 and 0.228 ± 0.005 eV $Å^{-1}$ for $(PDMA)PbBr_4$ and $(PDMA)PbI_4$, respectively. The slope of 0.078 ± 0.003 eV $Å^{-1}$ was obtained for $(BzA)_2PbI_4$, whereas 0.052 ± 0.01 and 0.036 ± 0.001 eV $Å^{-1}$ for $(BzA)_2PbBr_4$ below and above the isostructural phase transition, respectively (Figure 6a,b). This suggests a stronger dependency of the optical properties of PDMA systems on the change of the *a*-axis compared to the BzA systems. No correlation was observed between Pb–X–Pb angle and the optical absorption (Figure 6c,d), except in the case of isostructural phase transition regime in $(BzA)_2PbBr_4$ (Figure 6d). Thus, we find that the bandgap change is largely caused by the compression of the *a*-axis in the representative DJ and RP layered 2D perovskites, which is expected based on the reduced quantum confinement, whereas the changes do not correlate with the Pb–X–Pb angles within the same structural phase.

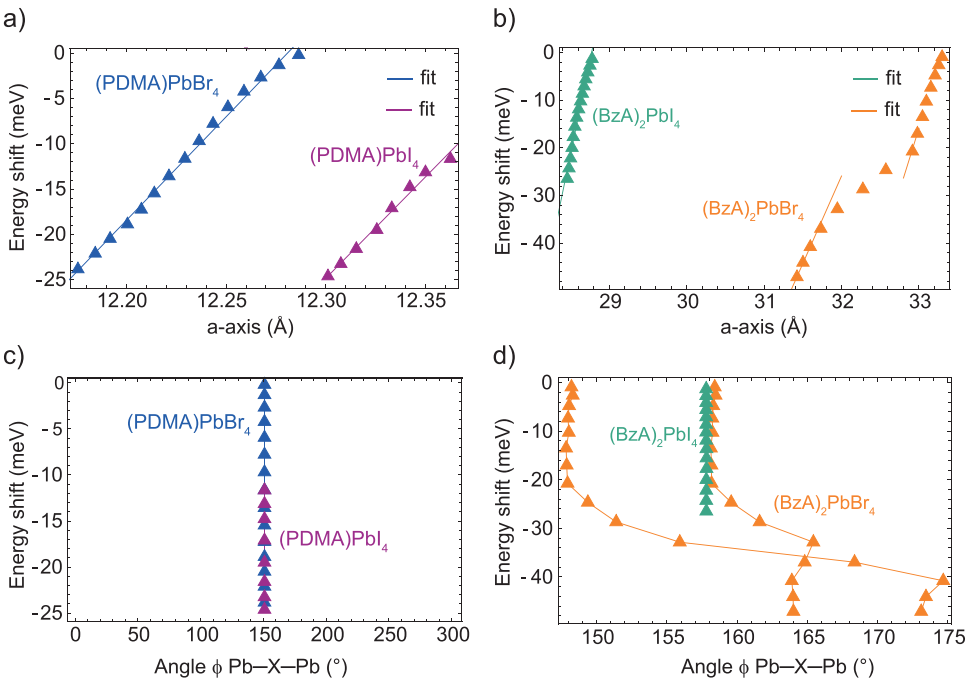

Figure 6. a,b) Optical absorption shift as a function of the *a*-axis length for the PDMA-system (a) and the BzA-system (b), and c,d) as a function of the Pb–X–Pb angles for the PDMA-system (c) and the BzA-system (d) based on the experimental data.

This further implies that the differences in the mechanochromic response for different organic moieties are associated with the interactions within the spacer layer and their contacts with the perovskite slabs.

Finally, the shifts of the excitonic peaks are fully recovered for both I- and Br-based RP and DJ perovskites upon decompression from 0.35 GPa to ambient pressure, implying that the process is reversible in this pressure range. The corresponding absorption spectra of both materials almost perfectly overlap after decompression (**Figure 7**a–d). The reversibility of the optical features strongly suggests structural reversibility, which is in agreement with the DFT predictions and in contrast with the amorphization commonly reported at higher pressures.[44–46] This reversibility of the mechanochromic response of layered hybrid perovskites is of interest to their use as model systems for elucidating structure–property relationships in hybrid layered materials. It is further relevant for the long-term stability of flexible perovskite devices and it points toward the use of mechanophores in the development of smart materials and pressure sensors.[47–49]

3. Conclusion

We report a direct comparison of the response of iodide and bromide-based RP and DJ 2D perovskites to pressure by using comparable aromatic spacer moieties, namely BzA and PDMA, respectively. We applied a mild pressure up to 0.35 GPa to all the compositions and detected a red shift of the excitonic peak upon increasing the pressure. Despite different binding mode of the spacers, we find that the RP and DJ perovskites behave similarly in this pressure range, with an anisotropic response predominantly in the out-of-plane (*a*-axis) direction. Moreover, while PDMA-based perovskites were not found to be susceptible to changes associated with the halide ion, presumably due to higher geometric constraints in DJ phases, BzA-based perovskite results in a larger excitonic peak shift in bromide-based compositions that is in contrast with their higher expected level of rigidity as compared to iodide-based phases. Furthermore, X-ray scattering experiments in conjunction with DFT calculations under pressure suggest that this effect is related to the structural properties of the 2D perovskite phases. Specifically, X-ray scattering experiments reveal significant relaxation of Pb–X–Pb angle in $(BzA)_2PbBr_4$, which is evidenced by the isostructural phase transition, whereas no phase transition is detected for the other compositions. DFT computations further indicate that this isostructural space group transition is associated with a decrease in the distance between BzA spacers and with an increased penetration depth of the spacers into the Pb–Br lattice. Moreover, this phase is the only one among the studied compositions that features a non-centrosymmetric lattice, which is likely to further amplify its mechanochromic response. These differences explain the large compression of $(BzA)_2PbBr_4$ under mild pressures. This study thereby provides important insights into the mechanochromic properties of layered hybrid perovskites while highlighting the importance of an interplay between the organic and the inorganic layers in the resulting structure. Moreover, the unique reversibility of their mechanochromic response in this mild pressure range opens a new perspective toward the utility of layered hybrid perovskites as potential platforms for amphidynamic materials[50,51] and mechanophores,[47–49] which expands the perspectives for their future applications.

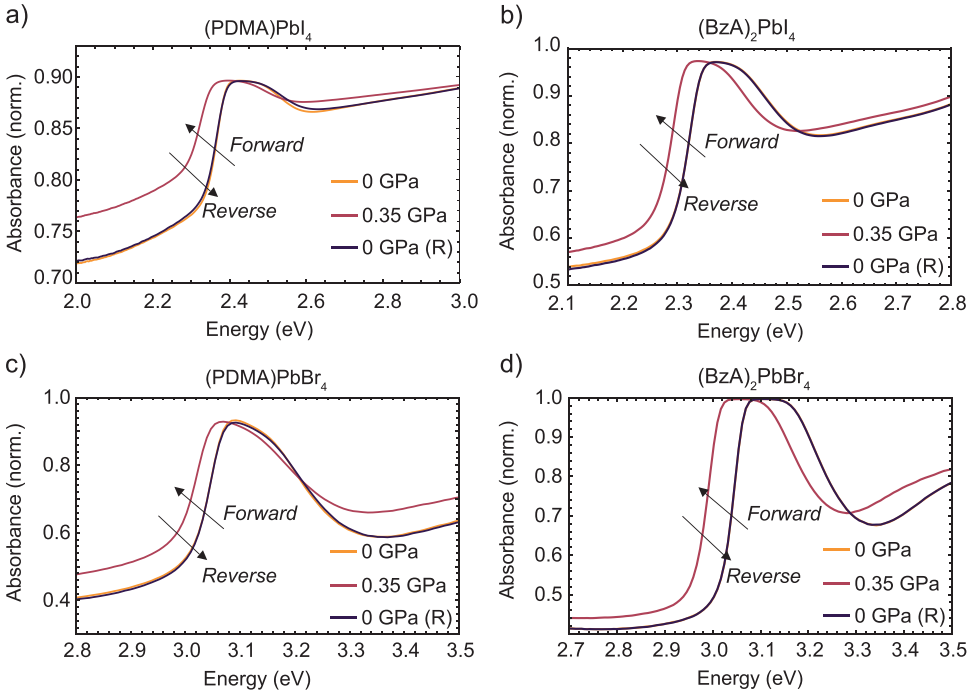

Figure 7. a–d) Pressure-dependent absorbance recorded using UV–vis at three characteristic pressures in the forward and reverse direction, for $(PDMA)PbI_4$ (a) $(BzA)_2PbI_4$ (b), $(PDMA)PbBr_4$ (c), and $(BzA)_2PbBr_4$ (d).

Supporting Information

Supporting Information is available from the Wiley Online Library or from the author.

Acknowledgements

The work of L.A.M. and B.E. was part of the Dutch Research Council (NWO) and was performed at the research institute AMOLF. The work of A.D. was supported by the EPFL-MPI Joint Research Center. B.E. and L.A.M. are grateful for the NWO Vidi grant 016.Vidi.179.005 and J.V.M. is grateful for the Swiss National Foundation PRIMA grant no. 19374 and NCCR Bio-Inspired Materials. U.R. acknowledges Swiss National Science Foundation Grant No. 200020-185092 and the NCCR-MUST for funding as well as computational resources from the Swiss National Computing Centre CSCS. The authors acknowledge Paul Scherrer Institute, Villigen, Switzerland for provision of synchrotron radiation beamtime at beamline X04SA of the SLS. The authors thank Juliane Borchert and Ya-Ru Wang (MPI-FKF) for commenting on the manuscript, Davide Moia (MPI-FKF) for his support, and Pascal Schouwink (EPFL) for the assistance in arranging structural measurements.

Open access funding provided by Universite de Fribourg.

Conflict of Interest

The authors declare no conflict of interest.

Author Contributions

L.A.M. and A.D. contributed equally to this work. The manuscript was written by L.A.M. and A.D. with the support of all co-authors, who led the project through efforts in experimental design, material preparation, and characterization. In particular, L.A.M. performed the measurements and the analysis of optoelectronic properties under pressure, while A.D. prepared the materials and conducted XRD measurements on thin films. M.D. performed the DFT calculations and structural characterization on the atomistic level and U.R. guided the computations and contributed to the interpretation of their results. M.A. and N.P.M.C. conducted the X-ray scattering measurements under pressure. J.M. and M.G. were involved in the discussion and supervision of A.D. throughout the study. The project was conceptualized by J.V.M. and B.E., who jointly directed the study. All authors contributed to and approved the final version of the manuscript.

Data Availability Statement

Data reported in this study can be accessed at https://doi.org/10.5281/zenodo.6285274 and https://doi.org/10.5281/zenodo.6323114 available under a CC-BY Creative Commons Attribution 4.0 International license.

Keywords

layered hybrid perovskites, mechanochromism, pressure-dependent optoelectronics

Received: October 29, 2021
Revised: February 8, 2022
Published online: March 20, 2022

[1] B. Saparov, D. B. Mitzi, *Chem. Rev.* **2016**, *116*, 4558.
[2] G. Grancini, M. K. Nazeeruddin, *Nat. Rev. Mater.* **2019**, *4*, 4.
[3] J. C. Blancon, J. Even, C. C. Stoumpos, M. G. Kanatzidis, A. D. Mohite, *Nat. Nanotechnol.* **2020**, *15*, 969.
[4] X. Li, J. M. Hoffman, M. G. Kanatzidis, *Chem. Rev.* **2021**, *121*, 2230.
[5] C. C. Stoumpos, D. H. Cao, D. J. Clark, J. Young, J. M. Rondinelli, J. I. Jang, J. T. Hupp, M. G. Kanatzidis, *Chem. Mater.* **2016**, *28*, 2852.
[6] L. Mao, W. Ke, L. Pedesseau, Y. Wu, C. Katan, J. Even, M. R. Wasielewski, C. C. Stoumpos, M. G. Kanatzidis, *J. Am. Chem. Soc.* **2018**, *140*, 3775.
[7] L. Kong, G. Liu, J. Gong, L. Mao, M. Chen, Q. Hu, X. Lü, W. Yang, M. G. Kanatzidis, H. K. Mao, *Proc. Natl. Acad. Sci. USA* **2020**, *117*, 16121.
[8] M. E. Kamminga, H.-H. Fang, M. R. Filip, F. Giustino, J. Baas, G. R. Blake, M. A. Loi, T. T. M. Palstra, *Chem. Mater* **2016**, *28*, 4554.
[9] L. Mao, C. C. Stoumpos, M. G. Kanatzidis, *J. Am. Chem. Soc.* **2018**, *141*, 1171.
[10] J. Blancon, A. V. Stier, H. Tsai, W. Nie, C. C. Stoumpos, B. Traoré, L. Pedesseau, M. Kepenekian, F. Katsutani, G. T. Noe, J. Kono, S. Tretiak, S. A. Crooker, C. Katan, M. G. Kanatzidis, J. J. Crochet, J. Even, A. D. Mohite, *Nat. Commun.* **2018**, *9*, 2254.
[11] J. A. Sichert, A. Hemmerling, C. Cardenas-Daw, A. S. Urban, J. Feldmann, *APL Mater.* **2019**, *7*, 041116.
[12] K. Zhang, M. Zhang, N. Zhu, H. Yin, J. Xing, L. Wang, *J. Mater. Sci.* **2021**, *56*, 11436.
[13] A. Jaffe, Y. Lin, H. I. Karunadasa, *ACS Energy Lett.* **2017**, *2*, 1549.
[14] S. Liu, S. Sun, C. K. Gan, A. G. Del Águila, Y. Fang, J. Xing, T. T. Ha Do, T. J. White, H. Li, W. Huang, Q. Xiong, *Sci. Adv.* **2019**, *5*, eaav9445.
[15] A. Jaffe, Y. Lin, C. M. Beavers, J. Voss, W. L. Mao, H. I. Karunadasa, *ACS Cent. Sci.* **2016**, *2*, 201.
[16] M. Szafrański, A. Katrusiak, *J. Phys. Chem. Lett.* **2017**, *8*, 2496.
[17] A. Jaffe, Y. Lin, W. L. Mao, H. I. Karunadasa, *J. Am. Chem. Soc.* **2015**, *137*, 1673.
[18] D. Umeyama, Y. Lin, H. I. Karunadasa, *Chem. Mater.* **2016**, *28*, 3241.
[19] Q. Li, L. Yin, Z. Chen, K. Deng, S. Luo, B. Zou, Z. Wang, J. Tang, Z. Quan, *Inorg. Chem.* **2019**, *58*, 1621.
[20] H. K. Mao, R. J. Hemley, J. F. Shu, L. C. Chen, A. P. Jephcoat, Y. Wu, *J. Geophys. Res.* **1991**, *96*, 8069.
[21] J. Kung, S. Rigden, *Phys. Chem. Miner.* **1999**, *26*, 234.
[22] G. Liu, J. Gong, L. Kong, R. D. Schaller, Q. Hu, Z. Liu, S. Yan, W. Yang, C. C. Stoumpos, M. G. Kanatzidis, H. kwang Mao, T. Xu, *Proc. Natl. Acad. Sci. USA* **2018**, *115*, 8076.
[23] Q. Tu, I. Spanopoulos, P. Yasaei, C. C. Stoumpos, M. G. Kanatzidis, G. S. Shekhawat, V. P. Dravid, *ACS Nano* **2018**, *12*, 10347.
[24] Q. Tu, I. Spanopoulos, S. Hao, C. Wolverton, M. G. Kanatzidis, G. S. Shekhawat, V. P. Dravid, *ACS Appl. Mater. Interfaces* **2018**, *10*, 22167.
[25] Q. Tu, I. Spanopoulos, E. S. Vasileiadou, X. Li, M. G. Kanatzidis, G. S. Shekhawat, V. P. Dravid, *ACS Appl. Mater. Interfaces* **2020**, *12*, 20440.
[26] G. Liu, L. Kong, P. Guo, C. C. Stoumpos, Q. Hu, Z. Liu, Z. Cai, D. J. Gosztola, H. K. Mao, M. G. Kanatzidis, R. D. Schaller, *ACS Energy Lett.* **2017**, *2*, 2518.
[27] K. Z. Du, Q. Tu, X. Zhang, Q. Han, J. Liu, S. Zauscher, D. B. Mitzi, *Inorg. Chem.* **2017**, *56*, 9291.
[28] L. Kong, G. Liua, J. Gong, Q. Hu, R. D. Schaller, P. Dera, D. Zhang, Z. Liu, W. Yang, K. Zhu, Y. Tang, C. Wang, S. H. Wei, T. Xu, H. K. Mao, *Proc. Natl. Acad. Sci. USA* **2016**, *113*, 8910.
[29] N. Ashari-Astani, F. Jahanbakhshi, M. Mladenović, A. Q. M. Alanazi, I. Ahmadabadi, M. R. Ejtehadi, M. I. Dar, M. Grätzel, U. Rothlisberger, *J. Phys. Chem. Lett.* **2019**, *10*, 3543.
[30] B. Guzelturk, T. Winkler, T. W. J. Van de Goor, M. D. Smith, S. A. Bourelle, S. Feldmann, M. Trigo, S. W. Teitelbaum, H. G. Steinrück, G. A. de la Pena, R. Alonso-Mori, D. Zhu, T. Sato,

H. I. Karunadasa, M. F. Toney, F. Deschler, A. M. Lindenberg, *Nat. Mater.* **2021**, *20*, 618.
[31] D. T. Limmer, N. S. Ginsberg, *J. Chem. Phys.* **2020**, *152*, 230901.
[32] C. Zhu, X. Niu, Y. Fu, N. Li, C. Hu, Y. Chen, X. He, G. Na, P. Liu, H. Zai, Y. Ge, Y. Lu, X. Ke, Y. Bai, S. Yang, P. Chen, Y. Li, M. Sui, L. Zhang, H. Zhou, Q. Chen, *Nat. Commun.* **2019**, *10*, 815.
[33] D. Liu, D. Luo, A. N. Iqbal, K. W. P. Orr, T. A. S. Doherty, Z. H. Lu, S. D. Stranks, W. Zhang, *Nat. Mater.* **2021**, *20*, 1337.
[34] Y. Chen, Y. Lei, Y. Li, Y. Yu, J. Cai, M. H. Chiu, R. Rao, Y. Gu, C. Wang, W. Choi, H. Hu, C. Wang, Y. Li, J. Song, J. Zhang, B. Qi, M. Lin, Z. Zhang, A. E. Islam, B. Maruyama, S. Dayeh, L. J. Li, K. Yang, Y. H. Lo, S. Xu, *Nature* **2020**, *577*, 209.
[35] C. Zhang, S. Wu, L. Tao, G. M. Arumugam, C. Liu, Z. Wang, S. Zhu, Y. Yang, J. Lin, X. Liu, R. E. I. Schropp, Y. Mai, *Adv. Energy Mater.* **2020**, *10*, 2002004.
[36] M. C. Gélvez-Rueda, P. Ahlawat, L. Merten, F. Jahanbakhshi, M. Mladenović, A. Hinderhofer, M. I. Dar, Y. Li, A. Dučinskas, B. Carlsen, W. Tress, A. Ummadisingu, S. M. Zakeeruddin, F. Schreiber, A. Hagfeldt, U. Rothlisberger, F. C. Grozema, J. V. Milić, M. Graetzel, *Adv. Funct. Mater.* **2020**, *30*, 2003428.
[37] S. Yu, Y. Yan, M. Abdellah, T. Pullerits, K. Zheng, Z. Liang, *Small* **2019**, *15*, 1905081.
[38] Y. Li, J. V. Milić, A. Ummadisingu, J. Y. Seo, J. H. Im, H. S. Kim, Y. Liu, M. I. Dar, S. M. Zakeeruddin, P. Wang, A. Hagfeldt, M. Grätzel, *Nano Lett.* **2019**, *19*, 150.
[39] L. Wang, K. Wang, G. Xiao, Q. Zeng, B. Zou, *J. Phys. Chem. Lett.* **2016**, *7*, 5273.
[40] T. Katsura, Y. Tange, *Minerals* **2019**, *9*, 745.
[41] A. Liang, S. Rahman, H. Saqib, P. Rodriguez-Hernandez, A. Muñoz, G. Nénert, I. Yousef, C. Popescu, D. Errandonea, *J. Phys. Chem. C* **2020**, *124*, 8669.
[42] N. Kitazawa, *Mater. Sci. Eng. B* **1997**, *49*, 233.
[43] X. Hong, T. Ishihara, A. U. Nurmikko, *Phys. Rev. B* **1992**, *45*, 6961.
[44] Y. Chen, R. Fu, L. Wang, Z. Ma, G. Xiao, K. Wang, B. Zou, *J. Mater. Chem. A* **2019**, *7*, 6357.
[45] Y. Qin, Z. Lv, S. Chen, W. Li, X. Wu, L. Ye, N. Li, P. Lu, *J. Phys. Chem. C* **2019**, *123*, 22491.
[46] L. Zhang, L. Wu, K. Wang, B. Zou, *Adv. Sci.* **2019**, *6*, 1801628.
[47] A. Al-Qatatsheh, Y. Morsi, A. Zavabeti, A. Zolfagharian, N. Salim, A. Z. Kouzani, B. Mosadegh, S. Gharaie, A. Z. K. Au, *Sensors* **2020**, *20*, 4484.
[48] J. Park, Y. Lee, M. H. Barbee, S. Cho, S. Cho, R. Shanker, J. Kim, J. Myoung, M. P. Kim, C. Baig, S. L. Craig, H. Ko, *Adv. Mater.* **2019**, *31*, 1808148.
[49] S. Cho, S. Kang, A. Pandya, R. Shanker, Z. Khan, Y. Lee, J. Park, S. L. Craig, H. Ko, *ACS Nano* **2017**, *11*, 7.
[50] W. Zhang, H.-Y. Ye, R. Graf, H. W. Spiess, Y.-F. Yao, R.-Q. Zhu, R.-G. Xiong, *J. Am. Chem. Soc* **2013**, *135*, 7.
[51] Y. L. Sun, C. Shi, W. Zhang, *Dalt. Trans.* **2017**, *46*, 16774.